



Biofilm microenvironment activated supramolecular nanoparticles for enhanced photodynamic therapy of bacterial keratitis



Haijie Han^{a,b,1}, Yifan Gao^{c,1}, Mengyin Chai^c, Xiaobo Zhang^{a,b}, Shaorui Liu^{a,b}, Yue Huang^c, Qiao Jin^c, Andrzej Grzybowski^{d,e}, Jian Ji^{c,*}, Ke Yao^{a,b,*}

^a Eye Center, the Second Affiliated Hospital, School of Medicine, Zhejiang University, 88 Jiefang Road, Hangzhou 310009, PR China

^b Zhejiang Provincial Key Lab of Ophthalmology, the Second Affiliated Hospital, School of Medicine, Zhejiang University, 88 Jiefang Road, Hangzhou 310009, PR China

^c MOE Key Laboratory of Macromolecule Synthesis and Functionalization of Ministry of Education, Department of Polymer Science and Engineering, Zhejiang University, Hangzhou 310027, PR China

^d Department of Ophthalmology, University of Warmia and Mazury, 60-554 Olsztyn, Poland

^e Institute for Research in Ophthalmology, Gorczyckiego 2/3, 61-553 Poznan, Poland

ARTICLE INFO

Keywords:

Biofilm microenvironment
Photodynamic therapy
Biofilms
Gram-negative bacteria
Bacterial keratitis

ABSTRACT

Infectious keratitis caused by bacterial biofilms is one of the main causes of corneal blindness, presenting a serious threat to public health. In this study, matrix metalloproteinase (MMP)-sensitive supramolecular nanoparticles (denoted as MMP-S NPs) were constructed for enhancing photodynamic antibacterial effect against biofilm-associated bacterial keratitis. MMP-S NPs were prepared by host-guest self-assembly of chlorin e6 (Ce6) conjugated β -cyclodextrin (β -CD) prodrug (β -CD-Ce6) and MMP-9-sensitive peptides (YGRKKRRQ-RRR-GPLGVRG-EEEEEE) terminated with adamantane (Ad) (Ad-MMP-S PEPs). MMP-S NPs with EEEEE peptide shell had a negatively charged surface, preventing adhesion to the normal ocular surface or healthy corneal cells, thus enhancing tear retention time. After arriving at the infected lesions, the protective EEEEE peptide shell of MMP-S NPs was removed, triggered by overexpressed MMP-9 in the keratitis microenvironment. The subsequently exposed cationic peptides helped the nanoparticles penetrate and accumulate in biofilms as well as bind to Gram-negative bacteria *Pseudomonas aeruginosa* (*P. aeruginosa*), which eventually improved the photodynamic antibacterial effect. Furthermore, the *P. aeruginosa* keratitis model verified the high effectiveness of a topical eye drop formulation of MMP-S NPs in killing bacteria by destroying the bacterial membrane as a result of *in situ* photodynamic activation of reactive oxygen species (ROS) formation under light irradiation. Moreover, the inflammatory response in the cornea was inhibited to a great extent. As a result, further damage to the corneal tissue was completely suppressed. This research provides a viable antibacterial alternative to fight against bacterial keratitis through effective elimination of infectious bacteria and eradication of bacterial biofilms in the cornea.

1. Introduction

As a sight-threatening ocular infection, bacterial keratitis is one of the main causes of corneal blindness. Bacterial keratitis often occurs after corneal trauma, wearing contact lenses, or the use of contaminated surgical instruments in ophthalmic surgery [1]. After exposure, pathogenic bacteria take the opportunity to invade the corneal tissue, causing a severe corneal inflammatory response [2,3]. Patients with bacterial keratitis therefore suffer from acute ocular pain, photophobia, lacrimation, blepharospasm, and decreased visual function. *Pseudomonas aeruginosa* (*P. aeruginosa*) keratitis is not only the most

common but also the most dangerous form of bacterial keratitis. It can destroy the whole cornea in 24–48 h and lead to loss of visual acuity, even blindness, within a few days [4]. Broad-spectrum antibiotics (e.g., levofloxacin and tobramycin) are usually topically administrated as first-line clinical treatment for bacterial keratitis. However, mounting evidence suggests that susceptibility to antibiotics is gradually decreasing as drug-resistant bacteria appear [5]. Meanwhile, a diverse range of bacteria, such as *P. aeruginosa*, form biofilms that are highly resistant to antibiotics, which makes curing corneal infections more and more challenging [6,7]. Hence, it is crucial to develop alternative therapeutic approaches for the management of bacterial keratitis.

* Corresponding authors.

E-mail addresses: jjjian@zju.edu.cn (J. Ji), xlren@zju.edu.cn (K. Yao).

¹ These authors contributed equally to this work.

Photodynamic therapy (PDT), discovered over 100 years ago, utilizes photosensitizers and light irradiation for generation of reactive oxygen species (ROS) to damage bacterial biological components and kill bacteria *via* oxidative stress [8,9]. PDT exhibits its efficacy in eliminating microorganisms, especially antibiotic-resistant microbial pathogens, by physically disrupting the cell membrane rather than interfering in metabolic processes [10–13]. However, as discussed earlier, many bacteria, including *P. aeruginosa*, can become resistant to traditional PDT due to the formation of biofilms [6,14,15]. Biofilms are mainly composed of water and extracellular polymeric substances (EPS), and the penetration of photosensitizers into biofilms can be severely hindered, leading to the failure of antibacterial PDT [12,16,17]. Furthermore, although most photosensitizers show strong antibacterial activity against Gram-positive bacteria, they are much less effective against Gram-negative bacteria owing to their permeability barrier constructed by cell envelope structures, which constrains the binding of photosensitizers [9].

Ligands, including sugar moieties and peptides, have been adopted to conjugate with photosensitizers to make PDT more effective against Gram-negative bacteria in biofilms [7,18–21]. Among these, cationic peptides can not only facilitate the penetration of photosensitizers into biofilms [8,12], but also have high affinity and specificity against Gram-negative bacteria, which can greatly improve the antimicrobial PDT of photosensitizers [9]. However, cationic peptides can also be non-specifically adsorbed to negatively charged host cells or even endogenous substances as a consequence of electrostatic interactions in nature [22–25]. In particular, when used for keratitis treatment, cationic peptides will interact with the negatively charged mucin distributed on the cornea, affecting the bacteria-targeting ability [26–28]. It is well documented that the microenvironment of biofilms is quite different from that of normal tissues [7]. For instance, matrix metalloproteinases (MMPs), such as MMP-9, are overexpressed in the bacterial biofilms and play a critical role in corneal melting [29–31]. Therefore, it will be particularly attractive to fabricate MMP-sensitive nanoparticles loaded with photosensitizers to improve the photodynamic antibacterial effect for biofilm-associated bacterial keratitis treatment.

To address these challenges, MMP-sensitive supramolecular nanoparticles (denoted as MMP-S NPs) with enhanced photodynamic antibacterial effects triggered by overexpressed MMP-9 in the biofilm environment were developed for treatment of corneal biofilms. These MMP-S NPs were fabricated *via* host-guest interactions between chlorin e6 (Ce6) conjugated β -cyclodextrin (β -CD) prodrug (β -CD-Ce6) and MMP-9-sensitive peptides (YGRKKRRQRRR-GPLGVRG-EEEEEE) terminated with adamantane (Ad) (Ad-MMP-S PEPs), in which Ad-MMP-S PEPs acted as the hydrophilic shell while Ce6 in β -CD-Ce6 acted as the hydrophobic core (Fig. 1). MMP-S NPs with EEEEE peptide shell had negatively charged surfaces and could avoid adhesion to normal ocular surfaces or healthy corneal cells, thereby enhancing tear retention time. After arriving at the sites of corneal infection, the protective EEEEE layer of MMP-S NPs was removed through cutting off GPLGVRG peptides by overexpressed MMP-9 in biofilms [32,33]. The subsequently exposed cationic peptides were expected to effectively promote the penetration and accumulation of MMP-S NPs into the biofilms as well as bind to *P. aeruginosa*, which eventually improved the antibacterial efficacy of PDT. Moreover, the inflammatory response in the cornea could be inhibited to a great extent, preventing further damage to the corneal tissue. Hence, MMP-S NPs are expected to exhibit superior PDT of bacteria elimination and biofilm eradication for efficient management of bacterial keratitis.

2. Materials and methods

2.1. Materials

β -CD and triethylamine were purchased from Sinopharm Co., Ltd. 1-(3-Dimethylaminopropyl)-3-ethylcarbodiimide hydrochloride (EDC) and

N-Hydroxysuccinimide (NHS) were provided by Aladdin Reagent Co., Ltd. Tosyl chloride (OTs), triethylenetetramine and amantadine (Ad) were supplied by Energy Chemical Co., Ltd. Chlorin e6 (Ce6) was supplied by J&K Scientific Ltd. 2',7'-Dichlorofluorescein diacetate (DCFH-DA), matrix 3-(4,5-dimethyl-thiazol-2-yl)-2,5-diphenyl tetrazolium bromide (MTT), metalloproteinases-9 (MMP-9) and mucin (from porcine stomach, type II) were purchased from Sigma-Aldrich. The designed guest molecules of MMP-9-sensitive peptides Ad-MMP-S PEPs and MMP-9-insensitive peptides Ad-YGRKKRRQRRR-GPMGMGRG-EEEEEE (Ad-MMP-IS PEPs) were custom-synthesized by Top-peptide Co., Ltd. MilliQ Water (18.2 M Ω /cm) was obtained using a Millipore MilliQ Academic Water Purification System. All other reagents and solvents were of analytical grade and used as received without further purification.

2.2. Characterizations

The ^1H NMR spectra were recorded on a Bruker DMX500 spectrometer. The size and zeta potential of the nanoparticles were measured by dynamic light scattering (DLS). DLS measurements were performed on Zetasizer Nano-ZS from Malvern Instruments equipped with a He–Ne laser (633 nm) at 25 °C. The morphology of the nanoparticles was observed by transmission electron microscopy (TEM) on a HT7700 TEM at an accelerating voltage of 80 kV. The fluorometric measurements were carried out using a Shimadzu RF-530 spectrometer. The fluorescence intensity was recorded at 525 nm with the excitation wavelength set as 488 nm. Fluorescence images were captured by Nikon DS-Ri2 fluorescence spectrometer. The morphology of bacteria was characterized by HITACHI S-4800 field emission scanning electron microscopy (SEM).

2.3. Synthesis of β -CD-Ce6

β -CD-Ce6 was obtained *via* a multistep synthesis routine according to our previous report [34] (Scheme S1). β -CD-OTs was first prepared by activating β -CD with tosyl chloride (OTs). In brief, 60 g of β -CD was dissolved in 250 mL of deionized water followed by adding sodium hydroxide solution (6.57 g in 15 mL of deionized water) dropwise. After β -CD was completely dissolved, the solution was placed into an ice bath. Then, OTs solution (16 g in 30 mL of acetonitrile) was added slowly while constantly stirring. Clear white precipitation appeared upon adding OTs. After further reacting for 4 h at room temperature, the mixture was placed into refrigerator overnight, recrystallized in water three times, and filtered to get the white product (β -CD-OTs). Next, β -CD-OTs was further reacted with triethylenetetramine to obtain β -CD-NH $_2$. One gram of β -CD-OTs was dissolved in 10 mL of dimethyl formamide, and then a mixed solution containing 1 mL of triethylamine and 0.8 mL of triethylenetetramine was added. The reaction was carried out for 72 h at 80 °C. The resultant solution was precipitated in acetonitrile three times followed by being dried in vacuum at 35 °C overnight to obtain β -CD-NH $_2$. Finally, 70 mg of β -CD-NH $_2$ was reacted with 25 mg of Ce6 under the catalysis of 30 mg of EDC and 20 mg of NHS in dimethyl sulfoxide (DMSO) for 24 h. Exhaustive dialysis (Mw = 1000) of the resultant was conducted against DMSO for 1 day and distilled water for 2 days. The β -CD-Ce6 conjugate was obtained *via* lyophilization.

2.4. Preparation and characterization of supramolecular nanoparticles

Ad-MMP-S PEPs solution (6 mg in 2 mL of deionized water) was added dropwise to the β -CD-Ce6 solution (3 mg in 2 mL of DMSO). The reaction mixture was then stirred for 24 h at room temperature in the dark, and MMP-sensitive supramolecular nanoparticles MMP-S NPs were obtained by spontaneous self-assembly of β -CD-Ce6 and Ad-MMP-S PEPs. The prepared nanocarriers were purified by dialysis (Mw = 3500) against deionized water for 2 days. MMP-insensitive supramolecular nanoparticles (denoted as MMP-IS NPs) were obtained

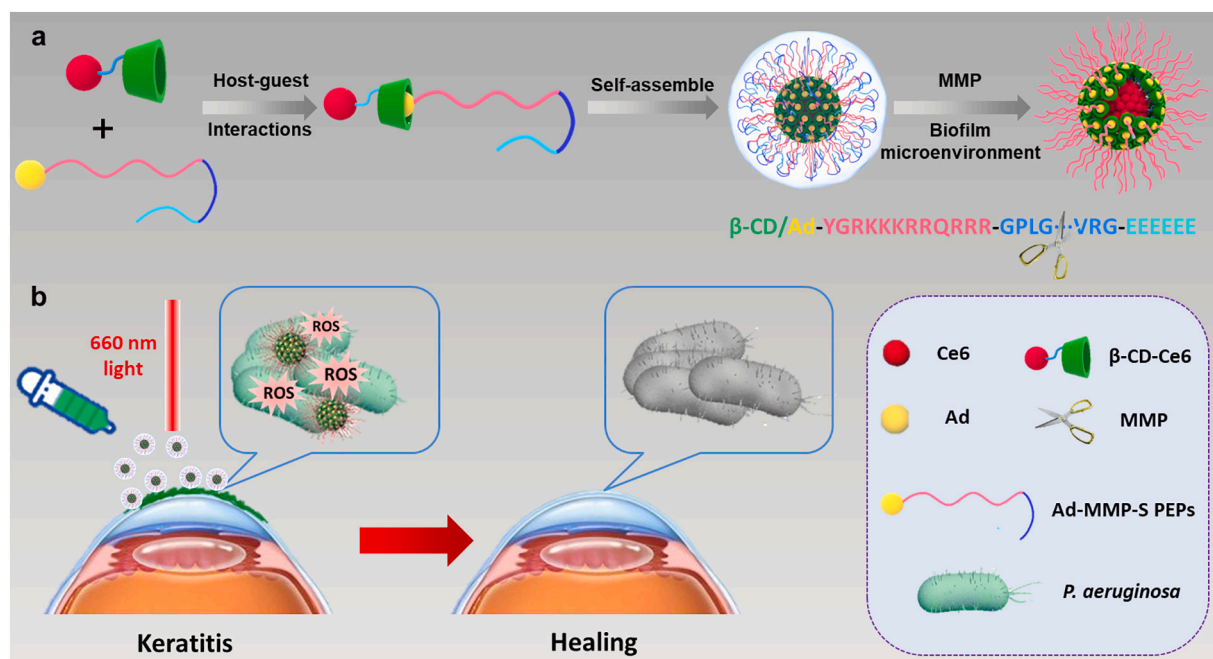


Fig. 1. (a) Schematic illustration of the preparation of MMP-S NPs and their MMP-sensitive behavior in biofilm microenvironment; (b) Schematics of MMP-activated enhanced antimicrobial PDT for cornea biofilm eradication via MMP-S NPs.

under the same conditions except using Ad -MMP-IS PEPs.

The formation of nanoparticles was characterized by measuring the diameter and observing the morphology through DLS and TEM. To confirm the MMP-9 cleavable ability of MMP-S NPs, phosphate-buffered saline (PBS; 10 mM, pH 5.0) and MMP-S NPs solution (100 μM Ce6 equivalent) were mixed with MMP-9 at a final concentration of 10 μM MMP-S NPs and 2 μg/mL MMP-9. After incubation at 37 °C for 4 h, the solution was taken out for zeta potential and hydrodynamic diameter measurements. Finally, to determine the Ce6 loading content of the nanoparticles, micellar solution was lyophilized and weighed, and Ce6 was subsequently measured using ¹H NMR and a Thermo Evolution 300 UV-Vis spectrophotometer at the wavelength of 405 nm.

2.5. The ROS generation of supramolecular nanoparticles *in vitro*

The ROS generation of supramolecular nanoparticles *in vitro* was measured using DCFH-DA as an indicator. DCFH-DA was first transformed to dichlorofluorescein (DCF) according to a reported procedure [35]. Then, 300 μL of supramolecular nanoparticles solution (10 μM Ce6 equivalent) was mixed with 100 μL dichlorofluorescein solution followed by 660 nm light irradiation (500 mW/cm² power) for 2 min. The supramolecular nanoparticles solution (10 μM Ce6 equivalent) without irradiation and PBS were also handled with the same process. Finally, the fluorescence intensity was recorded at 525 nm with the excitation wavelength as 488 nm.

2.6. Assessment of mucoadhesive properties

Mucoadhesive properties of MMP-S NPs and MMP-IS NPs were assessed by determining the turbidity of the mucin dispersion incubated with supramolecular nanoparticles according to previous reports [36]. Briefly, a freshly prepared mucin solution at a final concentration of 1 mg/mL was mixed with an equal volume of supramolecular nanoparticles at a final concentration of 500 μg/mL as well as MMP-9 at a final concentration of 2 μg/mL. This mixture was incubated in a thermostat incubator at 37 °C with constant shaking (100 rpm). Then, the spectrophotometric analysis was performed by recording the absorbance of the mixture at 600 nm with a UV-Vis spectrophotometer at

regular time points. The increase in turbidity of the sample, referring to mucin solution turbidity, indicated mucoadhesive properties. In addition, the absorbance of free mucin and MMP-9 was measured as controls.

2.7. Bacterial culture

P. aeruginosa and *Staphylococcus aureus* (*S. aureus*) were thawed from the −80 °C ultra-low temperature refrigerator and spread on agar plates by the plate streak method. After culture at 37 °C overnight, a certain amount of bacteria were scraped with an inoculating ring and cultured in Luria-Bertani (LB) at 37 °C on a shaker overnight. Subsequently, the bacteria were centrifuged (3000 RPM for 5 min) and washed with PBS three times. Finally, the bacteria were diluted to an appropriate number of colonies (colony forming units, CFU) for use.

2.8. Bacteria-targeting behavior of nanoparticles

A 100 μL of *P. aeruginosa* suspension (approximately 10⁸ CFU/mL) was mixed with 100 μL of micellar solution (10 μM Ce6 equivalent) in a 96-well plate and incubated in a 37 °C shaker for 4 h. Then, bacterial staining was performed with 50 μL of 4',6-diamidino-2-phenylindole (DAPI) solution. After standing for 15 min in the dark, the bacteria were washed with PBS three times, and the degree of adhesion of the nanoparticles to bacteria was subsequently observed by a fluorescence microscope.

2.9. Cell culture and cytotoxicity of nanoparticles

Human corneal epithelial cells (HCEs) were cultured using Dulbecco's Modified Eagle Medium/Nutrient Mixture F-12 (DMEM/F-12) containing 10% fetal bovine serum (FBS), 100 U/mL penicillin, and 100 mg/mL streptomycin at 37 °C in a humidified 5% CO₂ incubator.

The cytotoxicity of nanoparticles was studied using the MTT assay [37]. Briefly, HCEs in 180 μL of culture medium were seeded on a 96-well plate at a density of 6000 cells/well for 24 h. Then, 20 μL of MMP-S NPs solution was added to each well and incubated for another 4 h. After washed by PBS, the cells were treated with or without 660 nm

light irradiation (500 mW/cm² power) with different light irradiation times and further incubated for 24 h. Next, 20 µL of MTT (5 mg/mL) was added to each well, and the cells were further cultured at 37 °C for 4 h. Finally, the medium was replaced with 150 µL DMSO to dissolve the obtained crystals, and the OD values at 490 nm were measured using a microplate reader.

2.10. *In vitro* bactericidal activity of Ce6 and supramolecular nanoparticles

The standard plate counting method was utilized for evaluating the bactericidal activity of Ce6 and nanoparticles. First, 100 µL of *P. aeruginosa* or *S. aureus* suspension (about 10⁸ CFU/mL) was mixed with Ce6 or nanoparticles (10 µM Ce6 equivalent) in a 96-well plate. After shaking and incubating in a 37 °C shaker for 4 h, the samples were irradiated with a wavelength of 660 nm light and power of 500 mW/cm² for 0, 2, 4, and 8 min, respectively. Then, each sample was appropriately diluted and incubated with LB solid medium. Bacterial colonies were counted after 14 h of incubation at 37 °C. At the same time, the bacterial colonies of *P. aeruginosa* treated with nanoparticles in the dark were counted according to the aforementioned steps.

The morphologies of the bacteria treated with nanoparticles were investigated under a SEM. The bacteria suspension was incubated with MMP-S NPs solution (10 µM, calculated as Ce6). After shaking and incubating in a 37 °C shaker for 4 h, the samples were irradiated with a wavelength of 660 nm light and power of 500 mW/cm² for 0, 2, 4, and 8 min, respectively. Then, the suspension was dropped on a clear glass slide, fixed with glutaric dialdehyde for 2 h and dehydrated using graded ethanol (10%, 20%, 40%, 60%, 80%, and 100% for 10 min each). Gold was sputtered onto the samples before SEM tests.

2.11. The penetration and ROS generation behavior in biofilms

P. aeruginosa biofilms were cultured in glass dishes with LB broth at 37 °C. Two days later, the culture medium was removed, and the biofilms were gently washed with PBS before testing. The MMP-S NPs and MMP-IS NPs (30 µM, calculated as Ce6) were then added into the dishes. After 4 h of incubation, the biofilms were washed with PBS three times and further stained with DAPI. The fluorescence of the biofilms and the nanoparticles were visualized with confocal laser scanning microscopy (CLSM).

The ROS generation in *P. aeruginosa* biofilms was investigated using ROS indicator, DCFH-DA. Briefly, the *P. aeruginosa* biofilms were first cultured in 96-well plates. Then, PBS, MMP-S NPs (30 µM Ce6 equivalent), and MMP-IS NPs (30 µM Ce6 equivalent) was added into the biofilm, respectively. After 4 h of incubation, the biofilms were washed with PBS three times and further stained with DCFH-DA. The biofilms were irradiated by a 660 nm light (500 mW/cm² power) for 4 min and the fluorescence of DCF was visualized with fluorescent microscopy.

2.12. Antibacterial effects against biofilms

P. aeruginosa biofilms were cultured in 96-well plates for 2 days. Then, the culture medium was removed, and the biofilms were gently washed with PBS. The MMP-S NPs and MMP-IS NPs (30 µM, calculated as Ce6) were then added into each well. Four hours later, the samples were irradiated with a wavelength of 660 nm light and power of 500 mW/cm² for 0, 2, 4, and 8 min, respectively. PBS incubated biofilms were used as controls (CTRL). The biofilms were then dispersed by sonication for 10 min. Each sample was appropriately diluted and incubated with LB solid medium for plate counting.

2.13. Live/dead staining of biofilms

P. aeruginosa biofilms were cultured in glass dishes for 2 days. After washed with PBS, the biofilms were incubated with the nanoparticles

(30 µM, calculated as Ce6). The samples were irradiated using 660 nm light with a power of 500 mW/cm² for 4 min. Finally, the biofilms were stained with Live/Dead dye for 20 min and visualized with CLSM.

2.14. *P. aeruginosa*-infected keratitis induction and topical ocular eye drop administration

All animal procedures were performed in accordance with the ARVO (Association for Research in Vision and Ophthalmology) Statement for the Use of Animals in Ophthalmic and Vision Research and the Guidelines for Principles of Laboratory Animal Care (National Institutes of Health publication NO. 86–23, revised 1985). Twenty-five healthy C57BL/6 mice (5–6 weeks old and weighing approximately 18 g) were provided by the animal center of Zhejiang Academy of Medical Sciences. Bacterial inoculation was performed on the right corneas of the mice. The mice were topically anesthetized with 0.5% proparacaine hydrochloride (Alcaine; Alcon Laboratories, Inc.) followed by initiation of three 1 mm abrasions on the cornea using a 25-gauge needle. The mechanically damaged mice corneas were inoculated with 10 µL of *P. aeruginosa* suspension (about 10⁵ CFU/mL). After 12 h of inoculation, mice with infected eyes were randomly divided into five groups (CTRL, MMP-IS NPs + light, MMP-S NPs, MMP-S NPs + light, and LVFX) with five mice each. Specifically, three groups were instilled with 20 µL of MMP-IS NPs or MMP-S NPs (100 µM Ce6 equivalent) every 5 min for 6 cycles and then washed with 10 mL of normal saline. After 3 h of incubation, the corneas of the MMP-IS NPs + light and MMP-S NPs + light groups were irradiated with 660 nm light and an irradiation intensity of 250 mW/cm² for 5 min. The CTRL group was given normal saline only. The LVFX group was treated with commercially available levofloxacin eye drop (Tarivid®, Santen Pharmaceutical). All treatments were administered immediately from 12 h post-infection (H12). The MMP-IS NPs + light, MMP-S NPs, MMP-S NPs + light groups were administrated once and the LVFX group was continued for one consecutive week (four times daily).

2.15. Therapeutic efficacy evaluation

In order to investigate therapeutic efficacy, ophthalmic evaluations were performed by examining the infected eyes of mice following various treatments using slit-lamp biomicroscopy at 12 h, 1 day, 3 days, and 7 days after surgery. The clinical features of *P. aeruginosa* keratitis were scored and graded according to the previously reported literatures with a little modification [14,38]. A grade of 0 to 4 was assigned to each feature based on these three criteria: area of corneal opacity, density of opacity, and surface regularity. A normal untreated cornea was given a score of 0 in each category and thus had a total score of 0. The score for each eye could yield a possible total score ranging from 0 to 12. On behalf of determining the amount of viable bacteria in the infected cornea tissues, the excised corneas were homogenized in 0.5 mL of sterile PBS. Aliquots of 0.1 mL of 10-fold diluted samples were placed onto mannitol salt agar (MSA) plates. After incubation at 37 °C for 24 h, the colonies were counted and analyzed.

2.16. Histological analysis

At the end of the experiment, mice with different treatments were sacrificed, and their tissues were harvested. The tissues were then fixed in 4% paraformaldehyde in PBS, dehydrated in a graded series of ethanol solutions, embedded in paraffin, and cut into 5 µm-thick sections.

In order to investigate the histological changes and inflammatory response induced by the topical application of supramolecular nanoparticles or antibiotics, the mice corneal tissues were stained with hematoxylin and eosin (H&E), interleukin 1 beta (IL-1β), and tumor necrosis factor alpha (TNF-α) and examined visually under an optical microscope.

In order to evaluate the long-term effect of supramolecular nanoparticles or antibiotics on normal organs, major mice organs (liver, spleen, and kidneys) were stained with H&E and examined visually under an optical microscope.

2.17. Determination of blood parameters

At day 7, mice with different treatment were sacrificed and the blood samples were collected. The changes of white blood cell count (WBC), neutrophil count (NEUT), lymphocyte count (LYMPH), monocyte count (MONO), eosinophil count (EOS), red blood cell count (RBC), red hemoglobin count (HGB), hematocrit (HCT), and platelet count (PLT) in whole blood were measured. Serum levels of alanine aminotransferase (ALT), aspartate aminotransferase (AST), alkaline phosphatase (ALP), blood urea nitrogen (BUN), and creatinine (CREAT) were also investigated.

2.18. Statistical analysis

The results were expressed as the mean \pm standard deviation (SD). Analyses were performed using GraphPad Prism version 8.0 software. The difference between two groups was compared using Student's *t*-test. The difference was considered no significance as ns, statistically significant as $*p < 0.05$ and very significant as $**p < 0.01$.

3. Results and discussion

3.1. Preparation and characterization of supramolecular nanoparticles

β -CD-Ce6 was prepared via a multistep synthetic process (Scheme S1). In brief, β -CD was first activated with OTs to obtain β -CD-OTs and followed by treatment with excess triethylenetetramine to synthesize β -CD-NH₂. Finally, β -CD-Ce6 was acquired by an amidation reaction between β -CD-NH₂ and the lipophilic Ce6. One Ce6 was grafted onto one parental β -CD on average according to the ¹H NMR results (Fig. 2b). The MMP-9-cleavable peptides Ad-MMP-S PEPs with an Ad

termination were custom-synthesized and confirmed by mass spectrometry (MS) analysis (Fig. S2a). The non-cleavable peptides Ad-MMP-IS PEPs were used as the control (Fig. S2b). Based on the strong host-guest recognition between host molecule β -CD and guest molecule Ad, supramolecular nanoparticles MMP-S NPs with MMP-9-cleavable EEEEE peptide shell and MMP-IS NPs with uncleavable EEEEE peptide shell were obtained by the self-assembly of β -CD-Ce6 and MMP-9-sensitive peptide Ad-MMP-S PEPs or MMP-9-insensitive peptide Ad-MMP-IS PEPs, respectively.

Since MMP-9 is overexpressed in biofilm-associated bacterial (including *P. aeruginosa*) keratitis [7,29–31], the MMP-9 sensitive behavior of MMP-S NPs was first investigated. DLS was used to investigate the biofilm microenvironment-responsive size change of MMP-S NPs by incubation with MMP-9 at pH 5.0 to mimic the acidic biofilm microenvironment (pH 4.5–6.5) due to sugar fermentation [8,39]. As shown in Fig. 2c, the hydrodynamic diameters of MMP-S NPs and MMP-IS NPs were both 100 nm, which is favorable for the penetration of biofilm [40]. After incubation with MMP-9, the hydrodynamic diameter of MMP-IS NPs was almost unchanged while that of MMP-S NPs increased dramatically to over 1800 nm, which could achieve effective retention in biofilms. These results are consistent with previous reports that the stimulus-induced charge-reversal process may result in the occurrence of aggregation [41,42]. TEM was further applied to visually confirm this result. The obtained images revealed that MMP-S NPs had a spherical morphology with a diameter of approximately 60 nm, which was slightly smaller than that of the DLS results due to their dry form. After treatment with MMP-9, a larger and irregular morphology was observed, indicating the transformation of MMP-S NPs. Meanwhile, the surface charge of the nanoparticles after MMP-9 treatment was tested. As shown in Fig. 2d, the zeta potential of MMP-S NPs changed from -2.5 mV to $+7.3$ mV after MMP-9 treatment, indicating that the cationic peptide could be exposed after removal of the EEEEE peptide shell. Therefore, the MMP-S NPs can undergo surface charge reversal and size change process in the biofilm environment, which is beneficial for the penetration and long-term retention of MMP-S NPs in biofilms.

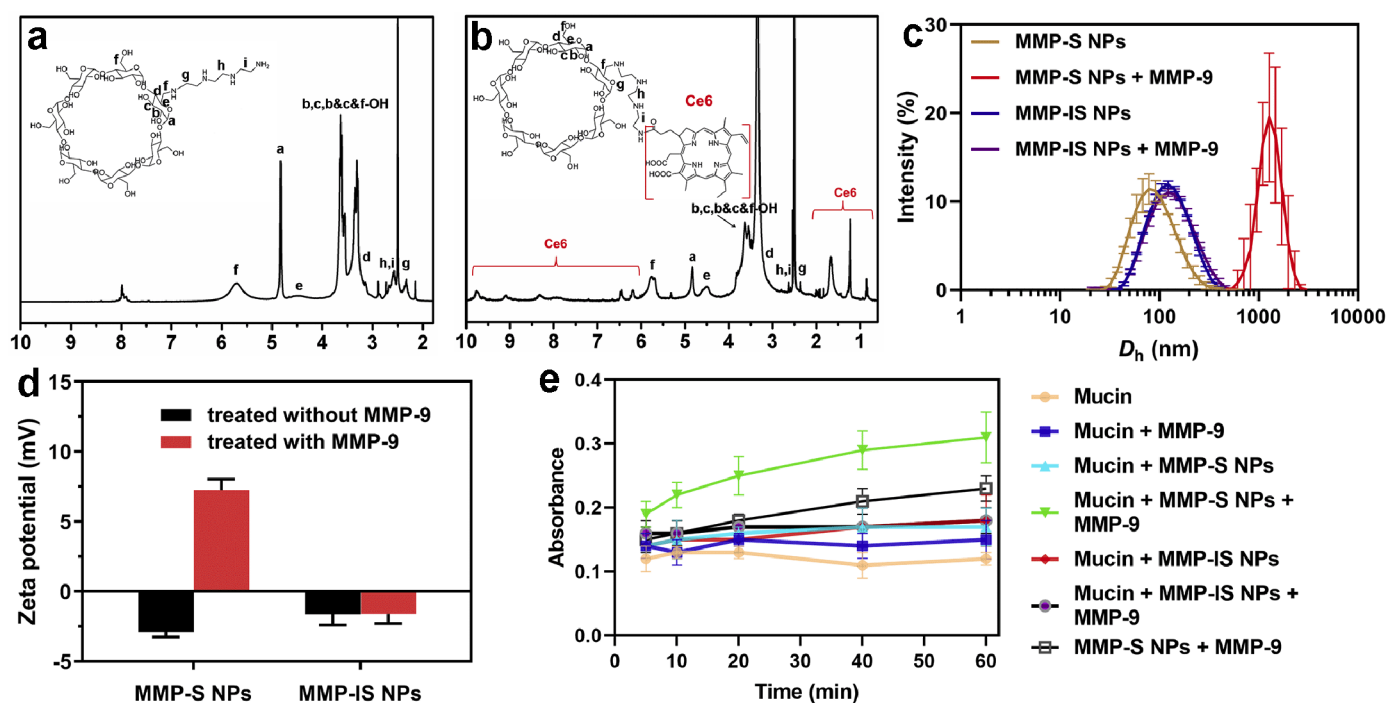


Fig. 2. Characterization of MMP-S NPs. ¹H NMR spectra of β -CD-NH₂ (a) and β -CD-Ce6 (b). Hydrodynamic diameter (c) and zeta potential (d) of MMP-S NPs and MMP-IS NPs treated with or without MMP-9. (e) Mucoadhesion studies by turbidimetric measurements.

3.2. Anti-mucoadhesive ability of the nanoparticles

Turbidimetric measurements were conducted to evaluate the anti-mucoadhesive ability of supramolecular nanoparticles by detecting the absorbance values of the mixture of selected nanoparticles and mucin at 600 nm. As shown in Fig. 2e, the absorbance values of the mixture of mucin and MMP-S NPs remained low, indicating superior anti-mucoadhesive ability because the EEEEE peptide could prevent interaction with mucin. The absorbance values of MMP-S NPs treated with MMP-9 had a slight increase owing to the MMP-9-responsive size increase. However, the absorbance values of mixtures of mucin and MMP-S NPs increased much more quickly and significantly during incubation with MMP-9 over time. The increase in turbidity revealed that cationic peptides of MMP-S NPs were exposed after treatment with MMP-9 and then interacted with negatively charged sialic acid residues of the mucin, resulting in aggregation [35]. In fact, this relevant feature of MMP-S NPs could enhance tear retention time by stopping mucoadhesion to the ocular surface and simultaneously enhancing the permeation of the biofilms activated by MMP-9 after arrival at the ulcer, thus guaranteeing accumulation of MMP-S NPs in the biofilms. In addition, the data showed that the absorbance values of MMP-IS NPs kept low during incubation with mucin dispersion, irrespective of whether MMP-9 were added, indicating excellent anti-mucoadhesive ability due to the uncleavable EEEEE peptide shell.

3.3. Bacteria-targeting behavior of MMP-S NPs

The targeting ligands of MMP-S NPs can be exposed, triggered by overexpressed MMP-9 in the infected sites. As a consequence, the nanoparticles bind to the bacteria due to electrostatic interactions with the anionic bacterial membrane, which is favorable for an efficacious PDT against bacteria. In order to investigate the targeting ability of nanoparticles, *P. aeruginosa* was incubated with MMP-S NPs and MMP-IS NPs at 37 °C for 4 h and collected by centrifugation. After labeling with DAPI, the fluorescence of bacteria was monitored using a fluorescence microscope. As shown in Fig. 3a, strong red fluorescence of Ce6 was clearly observed after *P. aeruginosa* was incubated with MMP-S NPs, demonstrating that MMP-S NPs effectively adhered to the bacteria in large quantities. It is deserved to mention that MMP-S NPs actually have stronger bacteria-targeting ability than the Fig. 3a shows, since the exposed cationic domains of MMP-S NPs can contact with other anionic substance in the culture media, which can interfere with the bacterial adhesion. In contrast, when *P. aeruginosa* was incubated with MMP-IS NPs that had an uncleavable EEEEE peptide shell, the red fluorescence of Ce6 was rather weak. Thus, it can be concluded that MMP-S NPs exhibit an enhanced Ce6 bacteria-targeting capability. The bacteria-targeting ability of the nanoparticles can enhance the local concentration of photosensitizers around bacteria and shorten the diffusion distance of easily deactivated ROS, which can largely enhance the PDT efficacy, especially for resistant Gram-negative bacteria.

3.4. In vitro bactericidal activity of Ce6 and supramolecular nanoparticles

The standard plate counting assay was performed to investigate the enhanced PDT activity of MMP-S NPs against *P. aeruginosa*. As shown in Fig. S4 and 3b, Ce6 exhibited good antibacterial activity against Gram-positive *S. aureus*, but was inefficient against Gram-negative *P. aeruginosa* due to its physical outer membrane barrier. Thus, MMP-S NPs were prepared to display MMP-9-activated improvements in the antibacterial activity of PDT against Gram-negative bacteria. After incubation with 10^8 CFU *P. aeruginosa* suspension for 4 h, MMP-S NPs eradicated more than 99.9% of *P. aeruginosa* with 4 min of 660 nm light irradiation (Fig. 3b). Prolonging the irradiation time could result in higher antibacterial efficacy as a consequence of enhanced ROS generation. Surprisingly, MMP-S NPs in the absence of light irradiation displayed a weaker but still clear bactericidal capacity by killing 89.1% of *P.*

aeruginosa. We supposed that the exposed cationic peptides could adhere to the bacterial membrane and destroy the membrane structure, leading to bacterial death. In contrast to MMP-S NPs, the antibacterial activity of MMP-IS NPs with light irradiation was much weaker since the MMP-IS NPs with uncleavable EEEEE peptide shell could hardly adhere to the outer membrane of *P. aeruginosa*; therefore, the PDT effect was limited. In addition, *P. aeruginosa* morphology after PDT treatment of MMP-S NPs was observed by SEM. As shown in Fig. 3d, compared to the PBS group, the bacterial morphology changed to an obvious irregular division when cells were irradiated for 8 min and the number of bacteria adhering to the substrate decreased significantly. It is noteworthy that MMP-S NPs revealed almost no cytotoxicity to HCEs with over 95% of cell viability under dark conditions, even at 50 μ M Ce6 equivalent, where the concentration of Ce6 was relatively high to bacteria, exhibiting good biocompatibility toward corneal epithelial cells (Fig. S5). Meanwhile, the cell viability of HCEs cells could still keep more than 80% in treatment with MMP-S NPs at a dosage of 30 μ M Ce6 with 8 min of 660 light irradiation (500 mW/cm² power), where the concentration of Ce6 and the irradiation intensity were much higher than the antibacterial experiments we adopted (Fig. S6). These results confirmed that biocompatible MMP-S NPs with light irradiation can enhance the antibacterial activity of Ce6 *in vitro*.

3.5. The penetration and ROS generation behavior in biofilms

P. aeruginosa keratitis results in biofilm formation on the cornea [14], thus limiting nanoparticles penetration of biofilms to eradicate the bacteria. Therefore, the penetration behavior of nanoparticles is particularly important for treating the biofilm-associated keratitis. Positively charged nanoparticles has been reported to be beneficial for improved penetration and accumulation in biofilms due to electrostatic interactions [8,12]. Since MMP-S NPs can undergo surface charge reversal in the biofilms of the infected sites, the penetration behavior of the nanoparticles was investigated. As shown in Fig. 4a, biofilms treated with MMP-S NPs showed strong red fluorescence of Ce6, which indicated an effective penetration and accumulation of the nanoparticles in *P. aeruginosa* biofilms. In contrast, only weak red fluorescence was detected for the MMP-IS NPs treated sample.

We further used ROS probe DCFH-DA to evaluate the ROS generation since the ROS production in biofilms directly affects the antibacterial efficiency. As shown in Fig. S7, without light irradiation, MMP-S NPs or MMP-IS NPs could not generate ROS as PBS. Under 660 nm light irradiation, both MMP-S NPs MMP-IS NPs could generate plentiful and almost equal amount of ROS. However, compared to the MMP-IS NPs group, much higher ROS generation of MMP-S NPs in biofilms was observed due to their better penetration and accumulation of NPs in biofilms, which can be ascribed to the surface charge reversal ability of the MMP-S NPs (Fig. S8). In the infected sites, the overexpressed MMP-9 can cut off GPLGVRG peptides and expose the cationic peptides, thus enhancing the penetration and retention of the nanoparticles, and ROS generation in biofilms.

3.6. Antibacterial effects against biofilms

The antibacterial effects of the nanoparticles against *P. aeruginosa* in biofilms were then evaluated. The living bacteria in biofilms were obtained and calculated using the standard plate counting assay after treatments (Fig. 4b and c). Unlike the results of the antibacterial tests against planktonic bacteria, MMP-S NPs (30 μ M, calculated as Ce6) did not cause bacterial death without irradiation, demonstrating the high resistance of the bacteria in biofilms. However, with 4 min of irradiation, a 99.4% reduction in bacterial survival rate was achieved, which illustrated the marvelous antibacterial ability of ROS. With a longer irradiation time of 8 min, the bactericidal rate of MMP-S NPs was observed to be as high as 99.997%, indicating that the nanoparticles may largely relieve the bacterial burden in the infected sites after

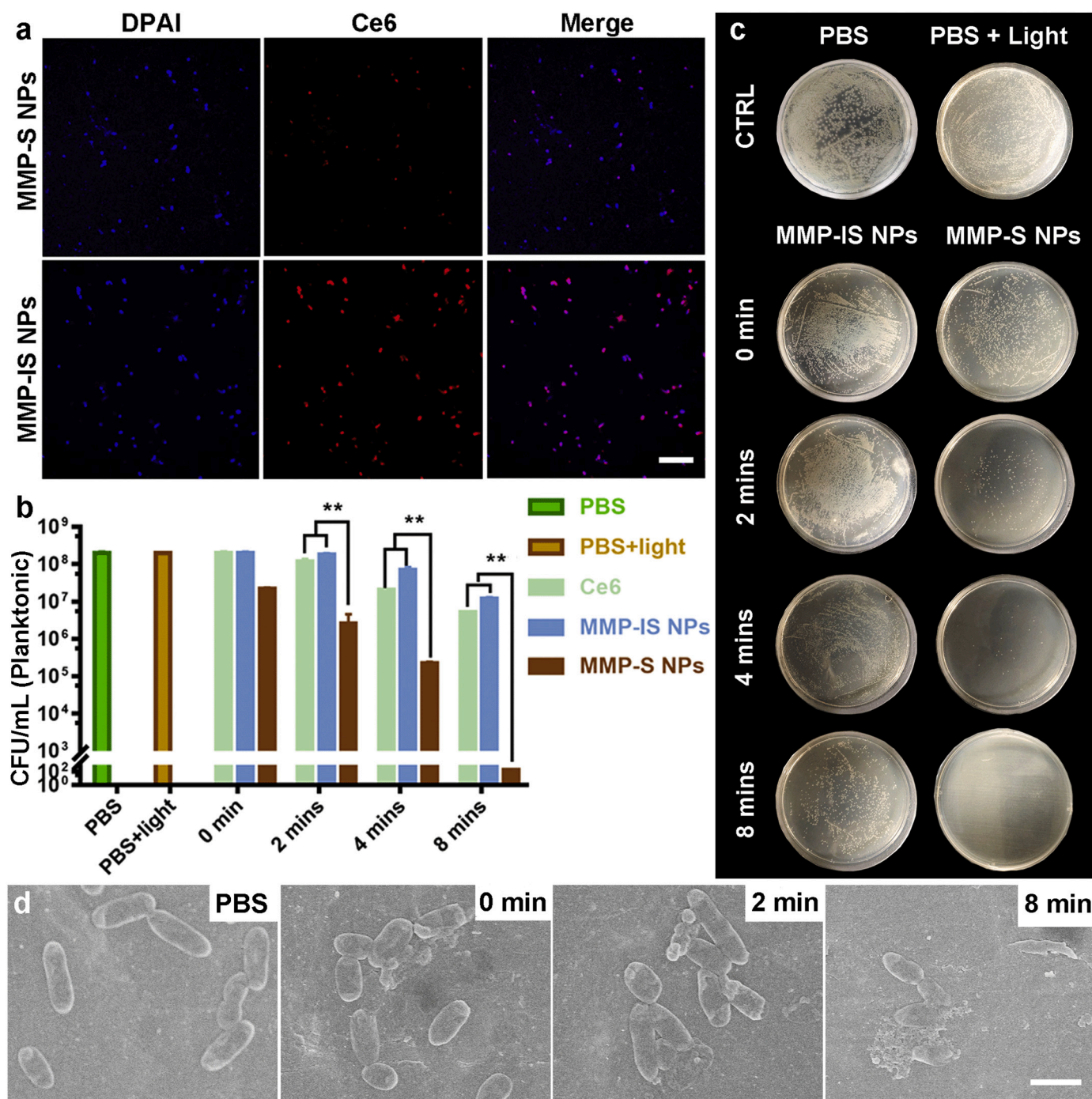


Fig. 3. Bactericidal performance evaluation of MMP-IS NPs and MMP-S NPs against planktonic *P. aeruginosa* in vitro. (a) Fluorescence microscopy images of *P. aeruginosa* incubated with MMP-IS NPs and MMP-S NPs at the concentration of 10 μM Ce6 for 4 h. The scale bar is 10 μm. (b) CFU of *P. aeruginosa* administrated with Ce6, MMP-IS NPs and MMP-S NPs at a dosage of 10 μM Ce6 (660 nm light and 500 mW/cm² power) with different irradiation times; **p* < 0.05 and ***p* < 0.01. (c) Representative photographs of the microorganisms. (d) SEM images of *P. aeruginosa* treated with MMP-S NPs at a dosage of 10 μM Ce6 (660 nm light and 500 mW/cm² power) with different irradiation times. The scale bar is 2 μm.

irradiation. In contrast, the antibacterial effects of the MMP-IS NPs were unsatisfactory due to limited biofilm penetration ability. A live/dead assay was also conducted to visualize the antibiofilm results (Fig. 4d). More red fluorescence was detected in the MMP-S NPs + light treated samples compared to the MMP-IS NPs + light treated samples, which further confirmed the greater antibacterial effects of MMP-S NPs against *P. aeruginosa* biofilms under light irradiation.

3.7. *P. aeruginosa* keratitis treatment

The experimental *P. aeruginosa*-infected keratitis models were first established and dedicated to evaluating the photodynamic antibacterial effect of current supramolecular nanoparticles. The anterior segment morphology after various topical ocular treatments was examined by slit-lamp microscopy, and relevant clinical scores were recorded. As shown in Fig. 5a, all of the mice corneas exhibited clinical signs of *P.*

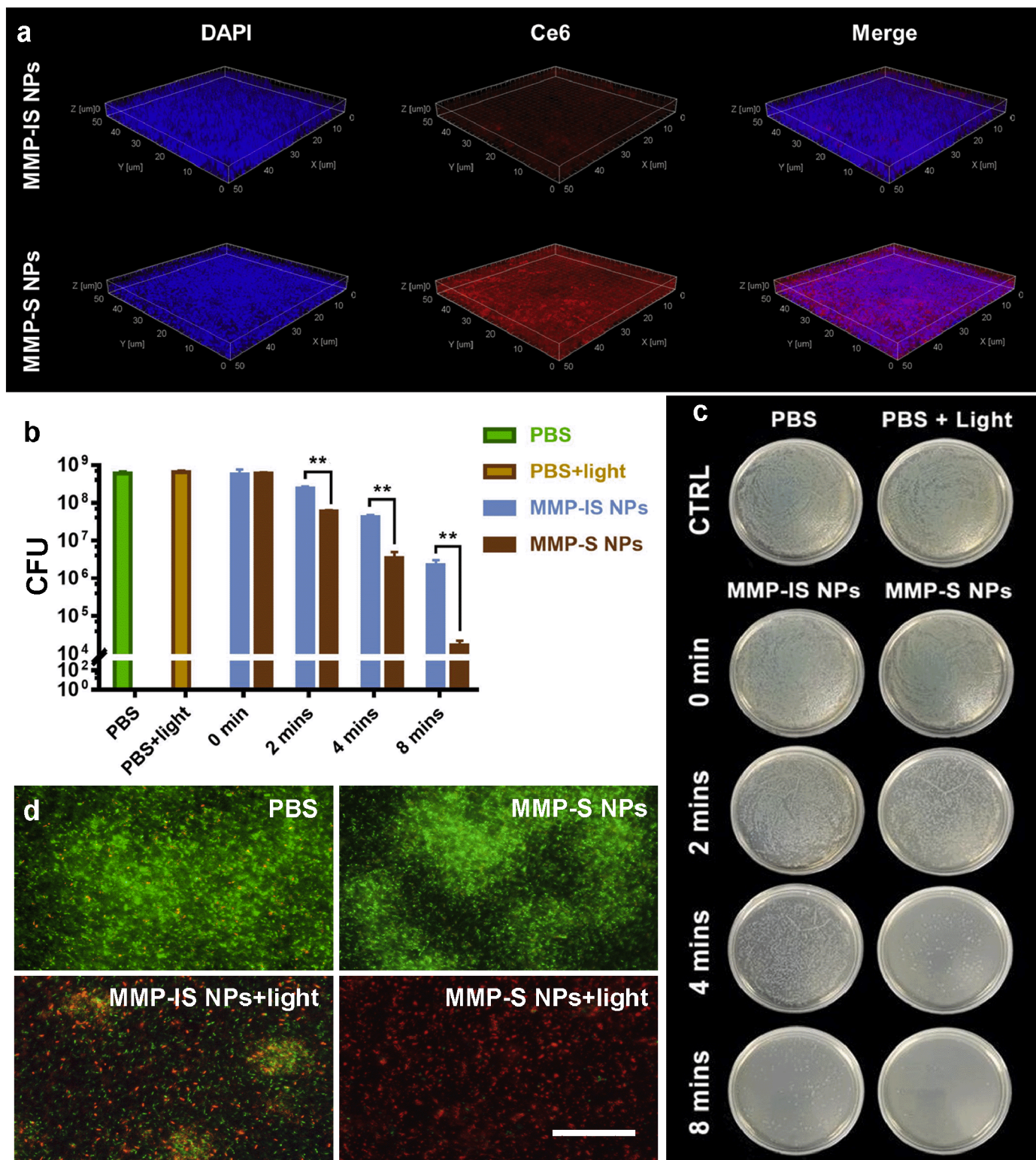
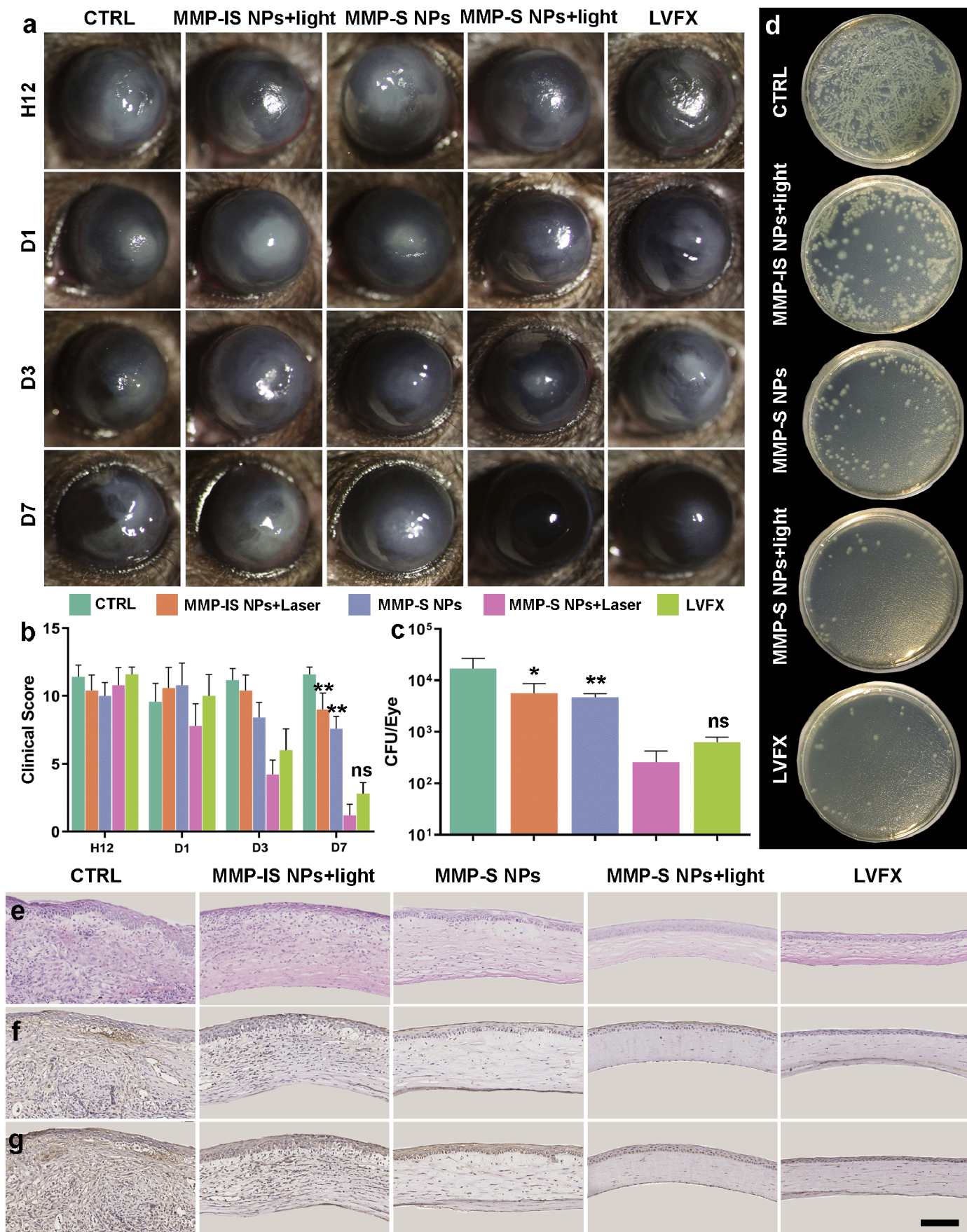


Fig. 4. Bactericidal performance evaluation of MMP-IS NPs and MMP-S NPs against *P. aeruginosa* biofilms. (a) Penetration behavior of nanoparticles in *P. aeruginosa* biofilms incubated with MMP-IS NPs and MMP-S NPs at the concentration of 30 μM Ce6 for 4 h. (b) CFU of *P. aeruginosa* administrated with MMP-IS NPs and MMP-S NPs at a dosage of 30 μM Ce6 (660 nm light and 500 mW/cm^2 power) with different irradiation times; * $p < 0.05$ and ** $p < 0.01$. (c) Representative photographs of the microorganisms. (d) Live/dead assay of *P. aeruginosa* biofilms treated with MMP-IS NPs and MMP-S NPs at a dosage of 30 μM Ce6 (660 nm light and 500 mW/cm^2 power) with 4 min of irradiation time. Bacteria were stained with SYTO 9 (green), and dead bacteria were stained with PI (red). The scale bar is 30 μm . (For interpretation of the references to colour in this figure legend, the reader is referred to the web version of this article.)



(caption on next page)

Fig. 5. Time-course *in vivo* therapeutic efficacy of the CTRL (sterilized saline), MMP-IS NPs + light (MMP-IS NPs upon light irradiation), MMP-S NPs (MMP-S NPs without light irradiation), MMP-S NPs + light (MMP-S NPs upon light irradiation), and LVFX groups in mouse corneas with experimental *P. aeruginosa*-infected keratitis (660 nm light and 250 mW/cm² power for 5 min). (a) Representative slit-lamp micrograph images of *P. aeruginosa*-infected keratitis treated with diverse therapies. (b) Corresponding quantified clinical score (0 to 12) based on three criteria (area of corneal opacity, density of opacity, and surface regularity). (c) Quantification of surviving *P. aeruginosa* in infected corneas. ns: no significance; **p* < 0.05 and ***p* < 0.01 vs. the MMP-S NPs + light group. (d) Photographs of bacterial colonies formed on LB-agar plates from the corneal tissues. Histopathologic and immunohistochemical photographs of rabbit corneas at day 7 after staining with H&E (e), IL-1 β (f), and TNF- α (g). The scale bar is 100 μ m.

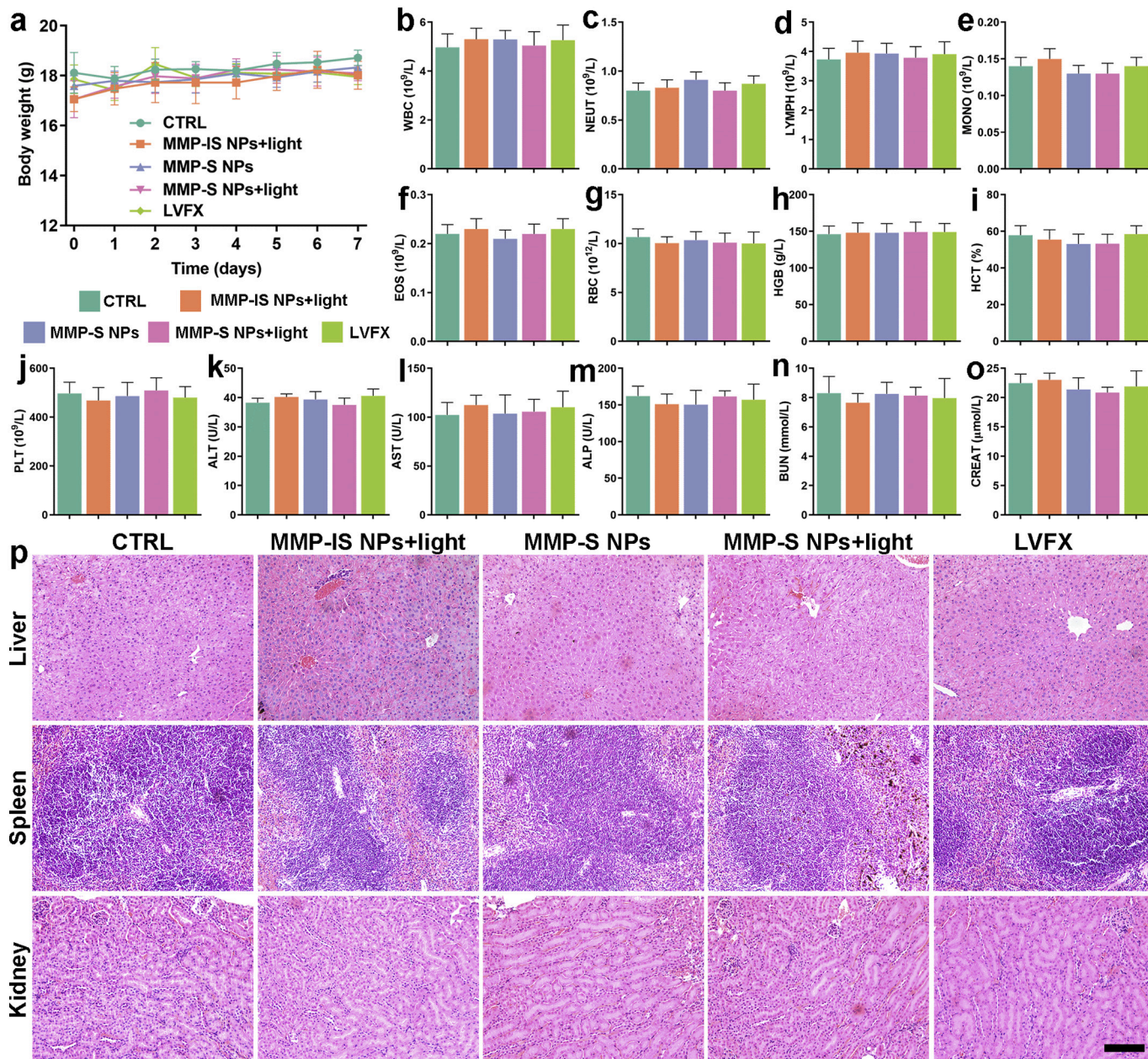


Fig. 6. Toxicity assessments. (a) Change in mouse body weight after diverse treatments. (b–j) Blood routine examination. WBC, white blood cell; NEUT, neutrophil; LYMPH, lymphocyte; MONO, monocyte; EOS, eosinophil; RBC, red blood cell; HGB, hemoglobin; HCT, hematocrit; PLT, platelet. (k–o) Blood biochemistry of the liver and kidneys. ALT, alanine transferase; AST, aspartate transferase; ALP, alkaline phosphatase; BUN, blood urea nitrogen; CREAT, creatinine. (p) Toxicological study via histological analysis of H&E staining of major organs, including the liver, spleen, and kidneys after different treatments at day 30 post-treatment. The scale bar is 100 μ m in all of the microscopy images. (For interpretation of the references to colour in this figure legend, the reader is referred to the web version of this article.)

aeruginosa infections with severe suppuration and dense opacity almost fully covering the cornea after 12 h post-infection and maintained a high total clinical score without significant differences. For the CTRL group, the *P. aeruginosa*-infected corneas continued to display severe ulcers in the 7 days following infection. After topical administration of MMP-IS NPs upon light irradiation (the MMP-IS NPs + light group),

infected cornea symptoms barely improved with a total clinical score of 9 because the MMP-IS NPs lacked a targeting ability due to the shielding of the uncleavable EEEEE peptide shell; therefore, the photodynamic antibacterial effect was restricted. Meanwhile, MMP-S NPs without light irradiation (the MMP-S NPs group) had a minimal positive effect on keratitis, similar to the MMP-IS NPs + light group, with a total

clinical score of 8. However, after topical administration of MMP-S NPs upon light irradiation (the MMP-S NPs + light group), the corneas markedly became clear and transparent, and the total clinical score decreased dramatically to 1 at day 7 post-infection, resulting in a statistical difference compared to the other two groups. The notably improved therapeutic effect of PDT may be attributed to the MMP-responsive enhanced penetration and retention of MMP-S NPs into biofilms of cornea. The shielding EEEEEEE peptide layer on MMP-S NPs was removed by overexpressed MMP-9 in biofilms, leading to the exposure of cationic peptides and subsequent penetration into biofilms and adhesion to the bacteria. Enhanced activity against *P. aeruginosa* was achieved as a result of the reduced distance between generated ROS and bacteria. It was also noteworthy that the LVFX group exhibited comparable therapeutic efficacy to the MMP-S NPs + light group, but the susceptibility of *P. aeruginosa* keratitis to antibiotics will be gradually decreasing in practice [5]. In addition, the host response to *P. aeruginosa* infection was studied by quantifying the number of surviving bacteria from the corneal tissues cultured on MSA plates overnight. Almost no colony formation was found in the MMP-S NPs + light and LVFX groups compared to the MMP-IS NPs + light and MMP-S NPs groups (Fig. 5c and d), further reflecting the superior antibacterial activity of the MMP-S NPs + light against *P. aeruginosa* corneal infection.

Furthermore, histological and immunohistochemical analyses of the infected corneas were performed after therapy (Fig. 5e, f and g). As is known, bacterial infections will cause stromal edema, infiltration of a large number of inflammatory cells (such as neutrophils), and disorganization of collagen fibrils. In the CTRL group, abnormal corneal architecture with heavy infiltration of inflammatory cells was observed in the *P. aeruginosa*-infected corneas. The inflammatory mediators, IL-1 β and TNF- α , were also highly expressed in the corneas. Furthermore, many infiltrated inflammatory cells were observed in the MMP-IS NPs + light and MMP-S NPs treated groups with a slight improvement compared to the CTRL group. In contrast, there were very few infiltrated inflammatory cells with limited expressions of IL-1 β and TNF- α in both the MMP-S NPs + light and LVFX treated groups. Moreover, the structure of the cornea was essentially restored to normal, the fibrous stromal layer was neatly arranged, and the three layers were clearly visible. Our findings suggested that MMP-S NPs under light irradiation had a similar therapeutic effect to commercial LVFX drops.

3.8. Toxicity assessments

Since the biocompatibility of the agents had an enormous impact on their potential clinical translation, a series of toxicity assessments, including mouse body weight, blood examinations, and histological analysis of major organs, were performed in this study. As shown in Fig. 6a, body weights of the mice in each group remained stable throughout the entire treatment process. Moreover, after topical ocular therapy, blood examination results, including blood index (WBC, NEUT, LYMPH, MONO, EOS, RBC, HGB, HCT, and PLT) and blood biochemistry of the liver and kidneys (ALT, AST, ALP, BUN, and CREAT), were normal (Fig. 6b–o). Furthermore, the long-term toxicity of supramolecular nanoparticles on major organs was studied by histological analysis. As displayed in Fig. 6p, no histopathological abnormalities or lesions in the liver, spleen, or kidneys were found at 30 days post-treatment. All of these toxicity assays verified the high biocompatibility of supramolecular nanoparticles, suggesting that they have great potential for future clinical application.

4. Conclusions

In summary, supramolecular nanoparticles MMP-S NPs with MMP-9 activated targeting ability were successfully prepared through host-guest interactions for efficient PDT against *P. aeruginosa* in biofilms. MMP-S NPs with EEEEEEE peptide shell had a negatively charged surface, protecting themselves from adhesion to the normal ocular surface

or healthy corneal cells and thus enhancing tear retention time. After arriving at the infected sites, the EEEEEEE peptide shell of MMP-S NPs was removed by cutting off enzyme-cleavable GPLGVRG peptides, which was triggered by overexpressed MMP-9. The subsequently exposed positively charged peptides were then ready to penetrate and accumulate in the biofilms, as well as adhere to *P. aeruginosa*, which eventually improved antibacterial efficacy of PDT. Furthermore, *P. aeruginosa* keratitis models verified the high effectiveness of a topical eye drop formulation of MMP-S NPs in killing bacteria by destroying the bacterial membrane as a result of *in situ* photodynamic activation of ROS upon light irradiation. Moreover, the corneal inflammatory response was greatly inhibited. As a result, further damage to the corneal tissue was completely suppressed. In this study, we provide a viable antibacterial alternative that can target the biofilm microenvironment to improve photodynamic antibacterial performance for the treatment of bacterial keratitis.

Declaration of Competing Interest

The authors declare no conflict of interest.

Acknowledgment

This research was supported by the Natural Science Foundation of China (Grant No. 81870641), National Key R&D Program of China (Grant No. 2018YFC1106104), Key Research and Development Program of Zhejiang Province (Grant No. 2020C03035), Zhejiang Province Natural Science Foundation (Grant No. LQ20E030011), Science and Technology Planning Project of Zhejiang Province (2016C04002) and Zhejiang Provincial Ten Thousand Talents Program (2018R52001).

Appendix A. Supplementary data

Supplementary data to this article can be found online at <https://doi.org/10.1016/j.jconrel.2020.09.014>.

References

- [1] S. Egrilmez, Ş. Yildirim-Theveny, Treatment-resistant bacterial keratitis: challenges and solutions, *Clin. Ophthalmol.* 14 (2020) 287–297.
- [2] L.E. Clemens, J. Jaynes, E. Lim, S.S. Kolar, R.Y. Reins, H. Baidouri, S. Hanlon, A.M. McDermott, K.W. Woodburn, Designed host Defense peptides for the treatment of bacterial keratitis, *Invest. Ophthalmol. Vis. Sci.* 58 (2017) 6273–6281.
- [3] A. Austin, T. Lietman, J. Rose-Nussbaumer, Update on the Management of Infectious Keratitis, *Ophthalmology* 124 (2017) 1678–1689.
- [4] A. Sy, M. Srinivasan, J. Mascarenhas, P. Lalitha, R. Rajaraman, M. Ravindran, C.E. Oldenburg, K.J. Ray, D. Glidden, M.E. Zegans, S.D. McLeod, T.M. Lietman, N.R. Acharya, *Pseudomonas aeruginosa* keratitis: outcomes and response to corticosteroid treatment, *Invest. Ophthalmol. Vis. Sci.* 53 (2012) 267–272.
- [5] L. Ung, P.J.M. Bispo, S.S. Shambhag, M.S. Gilmore, J. Chodosh, The persistent dilemma of microbial keratitis: global burden, diagnosis, and antimicrobial resistance, *Surv. Ophthalmol.* 64 (2019) 255–271.
- [6] W. Hou, X. Sun, Z. Wang, Y. Zhang, Biofilm-forming capacity of *Staphylococcus epidermidis*, *Staphylococcus aureus*, and *Pseudomonas aeruginosa* from ocular infections, *Invest. Ophthalmol. Vis. Sci.* 53 (2012) 5624–5631.
- [7] H. Koo, R.N. Allan, R.P. Howlin, P. Stoodley, L. Hall-Stoodley, Targeting microbial biofilms: current and prospective therapeutic strategies, *Nat. Rev. Microbiol.* 15 (2017) 740–755.
- [8] Y. Gao, J. Wang, M. Chai, X. Li, Y. Deng, Q. Jin, J. Ji, Size and charge adaptive clustered nanoparticles targeting the biofilm microenvironment for chronic lung infection management, *ACS Nano* 14 (2020) 5686–5699.
- [9] G.B. Kharkwal, S.K. Sharma, Y. Huang, T. Dai, M.R. Hamblin, Photodynamic therapy for infections: clinical applications, *Lasers Surg. Med.* 43 (2011) 755–767.
- [10] G. Su, Z. Wei, L. Wang, J. Shen, C. Baudouin, A. Labbé, Q. Liang, Evaluation of toluidine blue-mediated photodynamic therapy for experimental bacterial keratitis in rabbits, *Transl. Vis. Sci. Technol.* 9 (2020) 13.
- [11] H. Chen, J. Yang, L. Sun, H. Zhang, Y. Guo, J. Qu, W. Jiang, W. Chen, J. Ji, Y. Yang, B. Wang, Synergistic chemotherapy and photodynamic therapy of Endophthalmitis mediated by Zeolitic Imidazolate framework-based drug delivery systems, *Small* 15 (2019) 1903880.
- [12] D. Hu, Y. Deng, F. Jia, Q. Jin, J. Ji, Surface charge switchable supramolecular nanocarriers for nitric oxide synergistic photodynamic eradication of biofilms, *ACS*

- Nano 14 (2020) 347–359.
- [13] W. Huang, Q. Zhang, W. Li, M. Yuan, J. Zhou, L. Hua, Y. Chen, C. Ye, Y. Ma, Development of novel nanoantibiotics using an outer membrane vesicle-based drug efflux mechanism, *J. Control. Release* 317 (2020) 1–22.
- [14] A. Thanabalasuriar, B.N.V. Scott, M. Peiseler, M.E. Willson, Z. Zeng, P. Warrener, A.E. Keller, B.G.J. Surewaard, E.A. Dozier, J. TapioKorhonen, L.I. Cheng, M. Gadjeva, C.K. Stover, A. DiGiandomenico, P. Kubes, Neutrophil extracellular traps confine *Pseudomonas aeruginosa* ocular biofilms and restrict brain invasion, *Cell Host Microbe* 25 (2019) 526–536.
- [15] A. Antonoplis, X. Zang, M.A. Huttner, K.K.L. Chong, Y.B. Lee, J.Y. Co, M.R. Amieva, K.A. Kline, P.A. Wender, L. Cegelski, A dual-function antibiotic-transporter conjugate exhibits superior activity in sterilizing MRSA biofilms and killing Persister cells, *J. Am. Chem. Soc.* 140 (47) (2018) 16140–16151.
- [16] K. Forier, K. Raemdonck, S.C. De Smedt, J. Demeester, T. Coenye, K. Braeckmans, Lipid and polymer nanoparticles for drug delivery to bacterial biofilms, *J. Control. Release* 190 (2014) 607–623.
- [17] R.F. Landis, C. Li, A. Gupta, Y. Lee, M. Yazdani, N. Ngernyuan, I. Altinbasak, S. Mansoor, M.A.S. Khichi, A. Sanyal, V.M. Rotello, Biodegradable Nanocomposite antimicrobials for the eradication of multidrug-resistant bacterial biofilms without accumulated resistance, *J. Am. Chem. Soc.* 140 (2018) 6176–6182.
- [18] K.W. Jayawardana, H.S.N. Jayawardana, S.A. Wijesundera, T.D. Zoysa, M. Sundhoro, M. Yan, Selective targeting of *Mycobacterium smegmatis* with trehalose-functionalized nanoparticles, *Chem. Commun.* 51 (2015) 12028–12031.
- [19] A.K. Muszanska, E.T.J. Rochford, A. Gruszka, A.A. Bastian, H.J. Busscher, W. Norde, H.C. van der Mei, A. Herrmann, Antiadhesive polymer brush coating functionalized with antimicrobial and RGD peptides to reduce biofilm formation and enhance tissue integration, *Biomacromolecules* 15 (2014) 2019–2026.
- [20] S. Pescina, C. Ostacolo, I.M. Gomez-Monterrey, M. Sala, A. Bertamino, F. Sonvico, C. Padula, P. Santi, A. Bianchera, S. Nicoli, Cell penetrating peptides in ocular drug delivery: state of the art, *J. Control. Release* 284 (2018) 84–102.
- [21] G. Ferro-Flores, B. E. Ocampo-Garcia, L. Melendez-Alafort, Development of specific radiopharmaceuticals for infection imaging by targeting infectious micro-organisms, *Curr. Pharm. Des.* 18 (2012) 1098–1106.
- [22] Q. Jin, Y. Deng, X. Chen, J. Ji, Rational design of cancer nanomedicine for simultaneous stealth surface and enhanced cellular uptake, *ACS Nano* 13 (2019) 954–977.
- [23] D. Zhang, J. Wang, D. Xu, Cell-penetrating peptides as noninvasive transmembrane vectors for the development of novel multifunctional drug-delivery systems, *J. Control. Release* 229 (2016) 130–139.
- [24] M. Qiu, J. Ouyang, Y. Wei, J. Zhang, Q. Lan, C. Deng, Z. Zhong, Selective cell penetrating peptide-functionalized envelope-type chimaeric lipopepsomes boost systemic RNAi therapy for lung tumor, *Adv. Healthcare Mater.* 8 (2019) 1900500.
- [25] W. Yang, Y. Xia, Y. Fang, F. Meng, J. Zhang, R. Cheng, C. Deng, Z. Zhong, Selective cell penetrating peptide-functionalized Polymersomes mediate efficient and targeted delivery of methotrexate disodium to human lung Cancer in vivo, *Adv. Healthcare Mater.* 7 (2018) 1701135.
- [26] A. Sosnik, J. das Neves, B. Sarmento, Mucoadhesive polymers in the design of nano-drug delivery systems for administration by non-parenteral routes: a review, *Prog. Polym. Sci.* 39 (2014) 2030–2075.
- [27] H. Han, Q. Yin, X. Tang, X. Yu, Q. Gao, Y. Tang, A. Grzybowski, K. Yao, J. Ji, X. Shentu, Development of mucoadhesive cationic polypeptide micelles for sustained cabozantinib release and inhibition of corneal neovascularization, *J. Mater. Chem. B* 8 (2020) 5143–5154.
- [28] C. Jumelle, S. Gholizadeh, N. Annabi, R. Dana, Advances and limitations of drug delivery systems formulated as eye drops, *J. Control. Release* 321 (2020) 1–22.
- [29] K. Ikema, K. Matsumoto, Y. Inomata, Y. Komohara, S. Miyajima, M. Takeya, H. Tanihara, Induction of matrix metalloproteinases (MMPs) and tissue inhibitors of MMPs correlates with outcome of acute experimental pseudomonal keratitis, *Exp. Eye Res.* 83 (2006) 1396–1404.
- [30] E.C. Jamerson, A.M. Elhousseiny, R.H. ElSheikh, T.K. Eleiwa, Y.M. El Sayed, Role of matrix Metalloproteinase 9 in ocular surface disorders, *Eye Contact Lens* 46 (2020) S57–S63.
- [31] I. Vanlaere, C. Libert, Matrix metalloproteinases as drug targets in infections caused by gram-negative bacteria and in septic shock, *Clin. Microbiol. Rev.* 22 (2009) 224–239.
- [32] G. Qi, D. Zhang, F. Liu, Z. Qiao, H. Wang, An “on-site transformation” strategy for treatment of bacterial infection, *Adv. Mater.* 29 (2017) 1703461.
- [33] H. Han, D. Valdepérez, Q. Jin, B. Yang, Z. Li, Y. Wu, B. Pelaz, W.J. Parak, J. Ji, Dual enzymatic reaction-assisted gemcitabine delivery Systems for Programmed Pancreatic Cancer Therapy, *ACS Nano* 11 (2017) 1281–1291.
- [34] H. Tong, J. Du, H. Li, Q. Jin, Y. Wang, J. Ji, Programmed photosensitizer conjugated supramolecular nanocarriers with dual targeting ability for enhanced photodynamic therapy, *Chem. Commun.* 52 (2016) 11935–11938.
- [35] Y. Yuan, C. Zhang, B. Liu, A Photoactivatable AIE polymer for light-controlled gene delivery: concurrent Endo/Lysosomal escape and DNA unpacking, *Angew. Chem. Int. Ed.* 54 (2015) 11419–11423.
- [36] A. Račić, B. Čalijski, J. Milić, N. Milašinić, D. Krajišnik, Development of polysaccharide-based mucoadhesive ophthalmic lubricating vehicles: the effect of different polymers on physicochemical properties and functionality, *J. Drug Deliv. Sci. Tec.* 49 (2019) 50–57.
- [37] H. Han, Y. Hou, X. Chen, P. Zhang, M. Kang, Q. Jin, J. Ji, M. Gao, Metformin-induced stromal depletion to enhance the penetration of gemcitabine-loaded magnetic nanoparticles for pancreatic Cancer targeted therapy, *J. Am. Chem. Soc.* 142 (2020) 4944–4954.
- [38] M.H. Shih, F.C. Huang, Effects of photodynamic therapy on rapidly growing nontuberculous mycobacteria keratitis, *Invest. Ophthalmol. Vis. Sci.* 52 (2011) 223–229.
- [39] H. Flemming, J. Wingender, U. Szewzyk, P. Steinberg, S.A. Rice, S. Kjelleberg, Biofilms: an emergent form of bacterial life, *Nat. Rev. Microbiol.* 14 (2016) 563–575.
- [40] Y. Liu, L. Shi, L. Su, H.C. van der Mei, P.C. Jutte, Y. Ren, H.J. Busscher, Nanotechnology-based antimicrobials and delivery systems for biofilm-infection control, *Chem. Soc. Rev.* 48 (2019) 428–446.
- [41] H. Tian, Z. Guo, L. Lin, Z. Jiao, J. Chen, S. Gao, X. Zhu, X. Chen, pH-responsive zwitterionic copolypeptides as charge conversional shielding system for gene carriers, *J. Control. Release* 174 (2014) 117–125.
- [42] X. Deng, Y. Wang, F. Zhang, Z. Yin, Q. Hu, X. Xiao, Z. Zhou, Y. Wu, W. Sheng, Y. Zeng, Acidic pH-induced charge-reversal nanoparticles for accelerated endosomal escape and enhanced microRNA modulation in cancer cells, *Chem. Commun.* 52 (2016) 3243–3246.